Switching PID strategy for Positioning Systems with Non-Symmetric Friction and Noisy Velocity Measurements

Riccardo Lorigiola, Tommaso Borzone, Mattia Bruschetta and Angelo Cenedese

***Abstract*— This paper proposes a model-free, switching PID control strategy for point-to-point motion in positioning systems, where asymmetric friction and noisy velocity measurements are present. Traditional low-level control methods, such as PID, struggle with friction and noise in real-world conditions, particularly due to the difficulty in tuning parameters. The proposed approach employs a two-stage state-machine design to manage friction asymmetries and measurement noise, without requiring friction estimation or complex models. Experimental results on an industrial system demonstrate the approach's simplicity, robustness, and independence from system-specific parameters, offering a practical solution for high-precision, repeatable motion control in the presence of challenging disturbances.**

I. INTRODUCTION

In industrial applications, positioning systems are widely utilized and must provide high efficiency, precision, and movement repeatability. These systems are typically characterized by a motor, which transmits the motion via a series of gearboxes, moving a single-degree-of-freedom element. Due to the widespread, albeit implicit, need for fast movements combined with the handling of heavy components, these systems feature a relatively high reduction ratio. As a result, the load on mechanical elements, such as gear reducers and bearings, is considerable, causing disturbance phenomena. Indeed, as discussed in [1], [2], systems using long chains of gearboxes often suffer from induced vibrations and efficiency asymmetries. The other main critical aspect affecting system performance is the friction introduced by the mechanical components and the load on the system. In general, the modeling and characterization of friction have been extensively studied in the literature [3], [4] to improve the understanding of its effects and to develop compensation strategies within control systems.

The design of controllers that account for these disturbances is a well-established research focus in both industrial and academic settings. Given the constraints of industrial applications, highly complex control methodologies relying on model-based solutions or computationally expensive implementations are often impractical. Instead, simpler control strategies are preferred, particularly those that can be deployed on low-level embedded controllers. Among the most commonly used low-level controllers is the PID controller, which offers model-free control with high interpretability and robustness, depending on the tuning parameters. In the literature, PID controllers for point-to-point positioning have been often analyzed concerning friction phenomena to achieve high-precision and repeatable positioning control. For instance, in [6], the authors investigate the effects of undercompensation and overcompensation in PD point-to-point controllers with model-based static-friction compensation. The theoretical findings demonstrate that undercompensation results in system attraction toward a neighborhood of the desired position, whereas overcompensation can lead to limit cycles.

A promising approach for addressing position control challenges is presented in [7], which builds upon the results of [8], [9]. In [8], the authors provide a mathematical analysis of PID point-to-point control in the presence of Coulomb friction, proving global system convergence and bounded behavior under friction model perturbations. In [9], a reset PID control strategy for the same task is proposed to ensure global convergence to the desired equilibrium point, even in the presence of frictional weakening effects, commonly known as Stribeck effects. The proposed approach employs a state-machine-based reset mechanism that enables control action adjustments at specific instances, ensuring convergence both mathematically and experimentally. However, the effectiveness of this methodology is contingent upon the assumption of symmetric friction phenomena. Despite the reset strategy's independence from the precise knowledge of Stribeck function, an estimate of the static friction is required for its implementation. Furthermore, while theoretical guarantees exist regarding the avoidance of Zeno behavior through proper dwell-time selection, the practical interplay between static friction estimation, state-machine behavior, and velocity measurement noise poses challenges in parameter tuning, as shown and discussed in Section V.

In this paper, we propose a completely model-free switching PID strategy to achieve point-to-point motion in systems with asymmetric friction phenomena and noisy velocity readings. The switching strategy is performed using a two-stage state machine, where the switching between states is executed robustly using direct physical measurements. This approach eliminates the need for static friction estimation for the state machine or its interplay with dwell-time in noisy scenarios. The effectiveness of the proposed solution is then tested in a real industrial positioning system, where disturbance phenomena such as friction asymmetry and vibration are prominent. The results demonstrate the efficacy of the method, highlighting its simplicity and independence from

This work was supported by EniProgetti S.p.A.

R. Lorigiola, M.Bruschetta, A. Cenedese are with the Department of Information Engineering, University of Padua, via Gradenigo 6B, Padova, Italy riccardo.lorigiola@phd.unipd.it, mattia.bruschetta@unipd.it, angelo.cenedese@unipd.it

T. Borzone is with Robotics and Innovative Automation Systems, EniProgetti SpA, Venice, Italy tommaso.borzone@eni.com

Manuscript 985 submitted to 2025 64th IEEE Conference on Decision and Control (CDC). Received March 31, 2025.

system parameters for tuning.

II. PROBLEM FORMULATION

A. System dynamics and friction model

Consider the following generic dynamical system:

$$\dot{x} = v, \qquad m\dot{v} = u - u_f \tag{1}$$

where x, m, v, u, and u_f denote, respectively, the position, mass, velocity, control input, and friction force. In the subsequent discussion, all formulations are presented in terms of linear quantities, however, these expressions can be trivially extended to angular quantities by a straightforward change of notation.

Before formally defining the control problem, it is essential to discuss the modeling of the friction force u_f. The literature provides a broad range of friction models designed to capture different system configurations, component types, and operational characteristics [3], [4]. In general, friction models can be classified into two main categories: static models and dynamic models. Static friction models describe frictional behavior using set-valued functions of velocity, denoted as $v \rightrightarrows \Psi(v)$[1], which is typically defined as a case-dependent generalized-force function of velocity. Dynamic friction models, on the other hand, characterize friction using differential equations that introduce auxiliary states, generally fictitious and not related to physical quantities, to better represent the frictional evolution over time.

For this study, we adopt friction models that incorporate the Stribeck effect to describe the system's frictional behavior. In general, such models can be expressed as

$$v \rightrightarrows \Psi\left(v\right) := -F_s \,\mathrm{Sign}\left(v\right) - \alpha v + \psi\left(v\right) \tag{2}$$

$$\text{where } v\psi(v) \geq 0, \|\psi(v)\| \leq F_s,$$

$$\mathrm{Sign}(v) := \begin{cases} [\mathrm{sign}(v)] & \text{if } v \neq 0 \\ [-1, 1] & \text{if } v = 0 \end{cases}$$

where $\psi(v)$ represents a generic velocity-dependent weakening factor. A well-known example within this class of models is defined as

$$\Psi\left(v, F_{ext}\right) = \begin{cases} -\min\left(\|F_{ext}\|, F_s\right) \mathrm{sign}\left(F_{ext}\right) & \text{if } v = 0 \\ -\left(F_c + \left(F_s - F_c\right) e^{-\left(\frac{|v|}{v_s}\right)^{\delta\sigma}}\right) \mathrm{sign}(v) & \text{if } v \neq 0 \end{cases} \tag{3}$$

Fig. 1 provides a graphical representation of (3), facilitating a clear visualization of the previously discussed weakening effect.

To extend the set-valued function model (2) to asymmetric friction models, $v \rightrightarrows \Psi(v)$ in (2) can be reformulated as

$$v \rightrightarrows \Psi\left(v\right) := -\,\mathrm{Sign}_F\left(v\right) - \alpha v + \psi\left(v\right) \tag{4}$$

$$\text{where } v\psi(v) \geq 0, -F_s^- \leq \psi(v) \leq F_s^+,$$

$$\mathrm{Sign}_F(v) := \begin{cases} [F_s^+] & \text{if } v > 0 \\ [-F_s^-] & \text{if } v < 0 \\ [-F_s^-, F_s^+] & \text{if } v = 0 \end{cases}$$

[1]The symbol $\rightrightarrows$ specifically indicates that the function Ψ returns not a single value but sets.

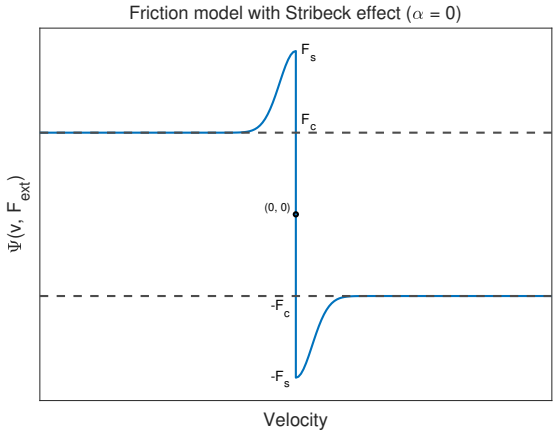

Fig. 1: Example of symmetric friction model (3). The Stribeck effect is evident in the peaks for low values of the velocity, after which the force remains constant at convergence values (corresponding to $\alpha = 0$ in (2)).

Therefore, by combining (1) and (4), and setting $m = 1$ without loss of generality, the system can be expressed as

$$\dot{x} = v, \qquad \dot{v} = u - \Psi(v) \tag{5}$$

Remark 1: Model (3) is employed exclusively for the experimental validation presented in Sections IV and V. Conversely, the theoretical proof and the analysis of the controlled system behavior utilize the set-valued function representation of the phenomenon (4).

B. Control problem

In this context, the control problem of interest requires to design a switching strategy for a PID controller to ensure convergence in point-to-point motion.

Before presenting the proposed solution, the PID control action and the complete system dynamics are introduced, with particular emphasis on the significance of the switching strategy in achieving the desired performance. For the sake of analytical tractability, the PID control action, which is generally defined as

$$u_{PID} = k_p(x_d - x) + k_i \int_0^t \left(x_d - x(\tau)\right) d\tau - k_d v, \tag{6}$$

where x_d represents the desired constant position, is rewritten as

$$\sigma = k_i \left(x_d - x\right), \tag{7a}$$

$$\phi = k_p \left(x_d - x\right) + k_i \int_0^t \sigma(\tau) d\tau, \tag{7b}$$

$$u = \phi - k_d \, v. \tag{7c}$$

or, equivalently, in its differential form

$$\dot{\sigma} = -k_i \, v, \qquad \sigma(0) = k_i \left(x_d - x(0)\right), \tag{8a}$$

$$\dot{\phi} = -k_p \, v + \sigma, \quad \phi(0) = k_p \left(x_d - x(0)\right) = \frac{k_p}{k_i}\sigma(0), \tag{8b}$$

$$u = \phi - k_d \, v. \tag{8c}$$

Manuscript 985 submitted to 2025 64th IEEE Conference on Decision and Control (CDC). Received March 31, 2025.

where σ represents the generalized position error, while ϕ denotes the controller state, which encapsulates both proportional and integral actions. Without loss of generality, but with a slight abuse of notation, setting $k_d = k_{d,PID} + \alpha$ and combining (4), (5), and (8), the overall system can be expressed as

$$\dot{\xi} = \begin{bmatrix} \dot{v} \\ \dot{\phi} \\ \dot{\sigma} \end{bmatrix} = \begin{bmatrix} -k_d & 1 & 0 \\ -k_p & 0 & 1 \\ -k_i & 0 & 0 \end{bmatrix} \begin{bmatrix} v \\ \phi \\ \sigma \end{bmatrix} + \begin{bmatrix} -\operatorname{Sign}_F(v) + \psi(v) \\ 0 \\ 0 \end{bmatrix} \quad (9)$$

From the previously defined system equation, it is possible to define the equilibrium set as

$$\mathcal{E} := \{\xi \in \mathbb{R}^3 : v = 0,\, \sigma = 0,\, -F_s^- < \phi < F_s^+\}. \quad (10)$$

In order to assure at least asymptotic convergence to the equilibrium point in the absence of friction ($F_s^+ = F_s^- = \psi(v) = 0, \forall v$), the evolution matrix in (9) is required to be Hurwitz.

Assumption 1: The parameters in (6), or equivalently in (7), are such that

$$k_p > 0,\, k_i > 0,\, k_p k_d > k_i$$

To provide clarity on the necessity of a switching action in the integral component included in by ϕ, a brief discussion is presented. During a stick phase, where $v = 0$, $\sigma(t) = \sigma$, and $-F_s^- \leq \phi \leq F_s^+$, the integral action in ϕ accumulates energy to overcome static friction in a specific direction. Once motion begins, if the resistance applied to the system, determined by the weakening factor $\psi(v)$, is lower than expected, i.e., less than F_s^- or F_s^+ in magnitude, an abrupt acceleration occurs. If these events occur near the equilibrium point, ϕ is discarded only after overshooting, resulting in moving away the system from the desired position. This sudden motion induces a hunting phenomenon around the desired position. Therefore, an ad hoc timed intervention in the integral action can effectively prevent hunting phenomena caused by the velocity-weakening factor.

III. SWITCHING PID

The proposed switching PID control action management is based on a state machine, which is represented by the state flow diagram in Fig. 2. Although the computation of the control action always follows (8), the switching of the integral term ϕ is regulated by this state machine.

By defining the augmenting system state as $\xi_e = \left[\xi^T, s\right]^T \in \mathbb{R}^3 \times \{1, -1\}$, it is possible to define the jump sets in (11) and the jump maps in (12), which govern the transitions in the state flow diagram.

$$\mathcal{D}_\sigma := \left\{\xi_e \in \mathbb{R}^3 \times \{1,-1\} : s = 1, \sigma = 0\right\} \quad (11a)$$
$$\mathcal{D}_v := \left\{\xi_e \in \mathbb{R}^3 \times \{1,-1\} : s = -1, v = 0\right\} \quad (11b)$$

$$g_\sigma(\xi_e) := \begin{bmatrix} v & -\phi & \sigma & -1 \end{bmatrix}^T \quad (12a)$$
$$g_v(\xi_e) := \begin{bmatrix} v & \sigma\frac{k_p}{k_i} & \sigma & 1 \end{bmatrix}^T \quad (12b)$$

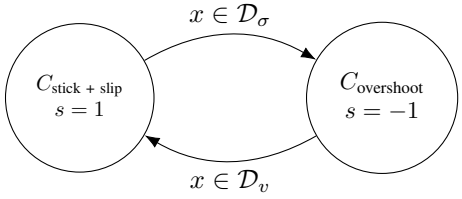

Fig. 2: Switching PID state machine

In addition, the equilibrium set in (10) can be extended to

$$\mathcal{E}_e := \{\xi_e \in \mathbb{R}^3 \times \{1,-1\} : v = 0,\, \sigma = 0, \\ -F_s^- < \phi < F_s^+, s \in \{1,-1\}\}. \quad (13)$$

Before presenting the proof of convergence for the proposed approach, some preliminary considerations are in order:

- The proposed flow set exhibits a continuous sequence of jumps without ever flowing only at the equilibrium set $\mathcal{E}$, ensuring that no dwell-time is required to prevent Zeno behavior. This characteristic arises from the integral relationship between the jump conditions on $\mathcal{D}_\sigma$ and $\mathcal{D}_v$.
- The control action does not incorporate any prior knowledge of the static friction values F_s^+ and F_s^-, as the jump maps impose no conditions on these parameters, relying solely on system measurements.
- From (4) and (8), it follows that when transitioning from $v = 0$ to $v \neq 0$, the term ϕ inherently exceeds the static friction threshold, thereby enabling system motion. Although this property is not explicitly enforced within the control design, it will be utilized in the Lyapunov analysis to establish the convergence of the controller.

Remark 2: Due to the control action and the switching strategy, the following inequalities are always satisfied throughout the entire motion of the system

$$s\phi v \geq 0, \quad \phi\sigma \geq 0 \quad (14)$$

The main technical result can now be stated as follows.

Theorem 1: The set $\mathcal{E}_e$ in (13) is globally asymptotically stable for (9) and the jump sets (11) and maps (12).

Proof: To prove the convergence of the proposed controller, the following hybrid discontinuous Lyapunov function $V(\xi_e)$ is employed:

$$V(\xi_e) = \frac{k_d}{k_i}\sigma^2 - 2\sigma v + k_p v^2 + \\ + (\operatorname{sign}(v)(\phi - s\phi^*))^2 + 2|\operatorname{sign}(v)|\frac{k_p}{k_i}s\phi^*\sigma \quad (15)$$

with

$$\phi^*(t_0) = \phi(t_0), \quad \begin{cases} \phi^*(t) = \phi(t) & \text{if } v = 0 \\ \frac{\mathrm{d}\phi^*}{\mathrm{d}t} = 0 & \text{if } v \neq 0 \end{cases} \quad (16)$$

As previously discussed, the additional term ϕ^* represents the value of the control action ϕ when the system begins to

Manuscript 985 submitted to 2025 64th IEEE Conference on Decision and Control (CDC). Received March 31, 2025.

move. Its behavior can be formally defined as in (16), where t_0 is the generic initial time instant when the system starts or when a transition occurs from $s = -1$ to $s = 1$.

Due to the symmetry of the Lyapunov function with respect to the movement of the system, i.e., $v \geq 0$ and $v \leq 0$, all the subsequent analysis is performed using the condition $v \geq 0$. Furthermore, it is trivial to prove that the proposed Lyapunov function is semi-definite positive, zero at the desired equilibrium set $\mathcal{E}_e$, and radially unbounded for $\xi_e \in \mathbb{R}^3 \times \{1, -1\}$.

Let us define t_0^+ such that $\sigma(t_0^+) > 0$, $v > 0$, and $\phi(t_0^+) \geq \frac{k_p}{k_i}\sigma(t_0^+)$. Since $v > 0$, the Lyapunov function is continuous, and thus its derivative can be computed.

Using Remark 2, (4) and (14),which implies

$$\phi^* \geq F_s^+ \implies \phi^* \geq F_s^+ + \psi(v),\ s\phi^*\sigma \geq 0 \tag{17}$$

it is possible to prove that $\frac{dV(\sigma_e)}{dt} < 0$ as shown hereafter, in (18):

$$\begin{aligned}\frac{dV(\sigma_e)}{dt} &= -2k_p\sigma v - 2\sigma\phi + 2\sigma\left(F_s^+ - \psi(v)\right) + 2k_d\sigma v \\ &\quad + 2k_i v^2 + 2k_p\phi v - 2k_p\left(F_s^+ - \psi(v)\right)v - 2k_p k_d v^2 + \\ &\quad - 2k_p\phi v + 2\sigma\phi + 2sk_p\phi^* v - 2s\phi^*\sigma - 2sk_p\phi^* v \\ &= 2\sigma\left(F_s^+ - \psi(v)\right) + 2v^2\left(k_i - k_p k_d\right) + \\ &\quad - 2k_p\left(F_s^+ - \psi(v)\right)v - 2s\phi^*\sigma \\ &< 2\sigma\left(F_s^+ - \psi(v)\right) - 2s\phi^*\sigma < 0\end{aligned} \tag{18}$$

In order to establish the convergence of the system to the equilibrium set $\mathcal{E}_e$, it is necessary to ensure that, in addition to $\frac{dV(\sigma_e)}{dt} < 0$, the Lyapunov function does not increase during jumps or discontinuities. By analyzing the jump maps, and considering that the Lyapunov function is quadratic, along with the conditions

$$\phi \geq \frac{k_p}{k_i}\sigma, \quad -s\phi\phi^* \leq 0$$

it is straightforward to demonstrate that the Lyapunov function remains non-increasing during jumps.

Regarding the discontinuity introduced by the sign function in the last two terms of the Lyapunov function, a different approach is used to establish the non-increasing property. Let t_0 and t_0^+ be time instants such that $v(t_0) = 0$ and $v(t_0^+) > 0$, with $\sigma(t_0^+)v(t_0^+) \approx 0$, $v^2(t_0^+) \approx 0$, and $\sigma(t_0) = \sigma(t_0^+)$. Similarly, let t_1^- and t_1 be time instants such that $v(t_1^-) > 0$, with $\sigma(t_1^-)v(t_1^-) \approx 0$, $v^2(t_1^-) \approx 0$, and $\sigma(t_1^-) = \sigma(t_1)$, while $v(t_1) = 0$. Using the results established in (18), the following chain of inequalities can be derived

$$\begin{aligned} & V\left(\xi_e(t_0^+)\right) > V\left(\xi_e(t_1^-)\right) \\ & \frac{k_d}{k_i}\sigma^2(t_0^+) + 2\frac{k_p}{k_i}|\phi^*(t_0^+)\sigma(t_0^+)| > \frac{k_d}{k_i}\sigma^2(t_1^-) + \left(\phi(t_1^-) - \phi^*(t_1^-)\right)^2 + \\ & \qquad + 2\frac{k_p}{k_i}|\phi^*(t_1^-)\sigma(t_1^-)| \\ & \qquad \cdots > \frac{k_d}{k_i}\sigma^2(t_1^-) + 2\frac{k_p}{k_i}|\phi^*(t_1^-)\sigma(t_1^-)| \\ \implies & 0 > \frac{k_d}{k_i}\left(\sigma^2(t_1^-) - \sigma^2(t_0^+)\right) + 2\frac{k_p}{k_i}\left(|\phi^*(t_1^-)\sigma(t_1^-)| - |\phi^*(t_0^+)\sigma(t_0^+)|\right) \\ \implies & |\sigma(t_1)| = |\sigma(t_1^-)| < |\sigma(t_0^+)| = |\sigma(t_0)| \\ \implies & V\left(\xi_e(t_0)\right) > V\left(\xi_e(t_1)\right) \end{aligned} \tag{19}$$

This proves that after a complete cycle of the state machine, the position error decreases. Therefore, despite the discontinuity introduced by the sign function, the overall system evolution leads to a monotonic decrement of the Lyapunov function. Consequently, since all elements contribute to reducing the Lyapunov function, the convergence to the equilibrium set $\mathcal{E}_e$ is assured. ■

Remark 3: To enhance robustness in real-world experiments and avoid the necessity of verifying strict equality conditions for the jump sets, a more robust formulation can be derived for $\mathcal{D}_\sigma$ and $\mathcal{D}_v$. By observing that $\mathcal{D}_\sigma$ identifies instances of system overshoot, equivalently to cases where the control action and the error are discordant, and that $\mathcal{D}_v$ detects conditions where the control action and the velocity are concordant, the jump sets in (11) can be rewritten as:

$$\mathcal{D}_\sigma := \left\{\xi_e \in \mathbb{R}^3 \times \{1, -1\} : s = 1, \phi\sigma \leq 0\right\} \tag{20a}$$

$$\mathcal{D}_v := \left\{\xi_e \in \mathbb{R}^3 \times \{1, -1\} : s = -1, \phi v \geq 0\right\} \tag{20b}$$

In addition, the proposed switching strategy exhibits intrinsic robustness to noisy velocity readings. Specifically, despite the possibility of incorrect $\mathcal{D}_v$-triggered jumps and frequent updates of ϕ^*, (19) remains valid when considering a complete cycle, which is ultimately governed by $\mathcal{D}_\sigma$. Thus, if accurate measurements of σ are available, a reasonable assumption, particularly in industrial applications, while velocity measurements are affected by noise, as observed in the analyzed settings, the proposed strategy remains effective.

This switching strategy has been demonstrated to successfully manage asymmetric friction models including the Stribeck effect, while maintaining robustness against noisy velocity readings, in a validation experimental campaign discussed in the following sections.

IV. EXPERIMENTAL SETUP

The setup consists of a single-degree-of-freedom (DOF) positioner operating against gravitational forces, displayed in Fig. 3. This type of positioner is widely utilized in industrial environments, frequently integrated with various automated systems to perform pick-and-place operations. Such positioners often serve as essential components in material handling, assembly, and other automated processes, where they are tasked with moving heavy loads while maintaining high precision despite the presence of disturbance factors such as friction phenomena.

The experimental setup comprises a DC motor driving a high-reduction-ratio gearbox, which moves a fixed load. The load is 70 kg, with the center of mass (CoM) located approximately 0.6 m from the joint, for a torque load of approximately 411.85 Nm. In the following, a detailed description of each component and its respective configuration is provided.

Actuator

The actuator utilized in this study (white element in Fig. 3) is a Maxon EC45 DC servo motor (Maxon EC45 datasheet). The motor is regulated via an `ELMO` motor control driver, using `SimplIQ` language via serial communication.

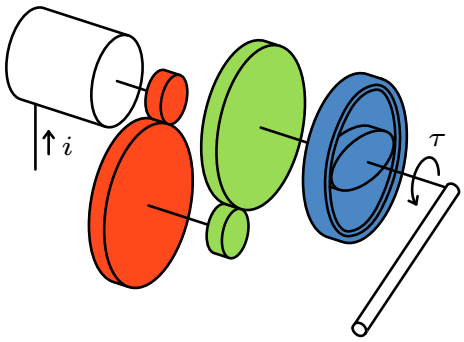

Fig. 3: Reset state machine proposed in [7]

Through this interface, a current reference can be provided, while the driver autonomously manages the actual current regulation via an internal current control loop. Table I reports some relevant motor data and communication settings.

TABLE I: Actuator parameters

Motor	
Torque constant	36.9 mNm/A
Maximum current ($i_{\max}$)	2.0 A
Maximum angular velocity ($\omega_{\max}$)	5000 rpm
Communication	
Baud rate	57600 baud
End character	';'
Reading timeout	1000 ms
Buffer size	256 byte

Gearbox

Given the operational requirements of positioner systems, which frequently handle heavy loads, the system is equipped with a three-stage reduction gearbox designed to enhance output torque while simultaneously decreasing system velocity. The three distinct stages of the gearbox can be clearly identified in Fig. 3 through the use of color coding.

The first two stages consist of gear reductions: the initial stage (red) is an 18:1 Maxon motor reduction, and the second stage is a custom-built gear reducer with a ratio of 10.1:1. The final stage (blue) features a commercially available HFUC-2A Harmonic Drive, which provides a reduction ratio of 160:1 (HFUC-2A Harmonic Drive datasheet). Due to the use of this long chain of gearboxes, as reported in [1] and [2], vibration within the system and asymmetry depending on the motion direction arises. In addition, due to lubrication phenomena, specific system configurations, and temperature variations, these parameters may fluctuate, resulting in unknown changes in the friction model.

Encoder

The angular position of the system is determined using an absolute encoder mounted at the output end of the gearbox reduction stage, i.e. slow shaft. The encoder employed is the E201-9B, a high-precision 20-bit device that communicates via the `RS-232` serial communication protocol. Table II presents the key specifications and communication settings of the encoder.

TABLE II: Encoder parameters

Encoder	
Precision	20 bit
$\Delta\vartheta$	$360°/2^{20} \approx 0.000343°$
$\sigma(std)$	$0.00029952°$ (experimental)
Communication	
Baud rate	2000000 baud
Reading char	'4'
Response from reading request	16 byte
Thread running time	0.1 ms

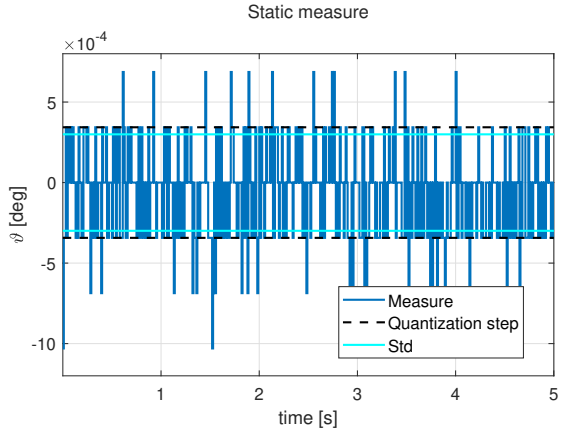

Fig. 4: Encoder static positioning measure

Fig. 4 illustrates the measurements obtained during a static positioning test, with the encoder sampled at a frequency of 100 Hz. The results indicate that the observed standard deviation closely corresponds to the quantization error inherent to the encoder, highlighting the device's measurement resolution and precision.

A. Gravity compensation and friction analysis

The system under consideration is characterized by an important impact of gravity on the friction phenomenon: the gravitation component combined with the high payload results in strongly asymmetric friction. Despite the proposed switching PID controller is proved to ensure global convergence to $\mathcal{E}_e$ even in the presence of asymmetric friction phenomena, we introduced gravity compensation to symmetrize the friction force effect, aligning with the conventional approach used in similar contexts when no dedicated strategy, like the one proposed, could be applied.

In order to eliminate dynamic effects due to the friction model, constant velocity ω_d experiments are conducted using a velocity PID controller with the control action $u_{vel,PID}$. In this way, the control action in these experiments precisely compensates for both the gravitational term and the friction force. Since the objective is to compare with controllers that assume symmetric static friction, the friction model in (2) is adopted, leading to the following equality

$$\begin{aligned} u_{vel,PID} &= k_g \cos(\vartheta) - \Psi\left(v, F_{ext}\right) \\ &= k_g \cos(\vartheta) + \begin{cases} \min\left(\|F_{ext}\|, F_s\right) \operatorname{sign}\left(F_{ext}\right), & \text{if } v = 0, \\ \left(F_c + \left(F_s - F_c\right) e^{-\left(\frac{|v|}{v_s}\right)^{\delta_\sigma}}\right) \operatorname{sign}(v), & \text{if } v \neq 0. \end{cases} \end{aligned} \tag{21}$$

By optimizing the experimental results using mean squared error (MSE) techniques, the estimated parameters are obtained as:

$$\left[\hat{k}_g, \hat{F}_c, \hat{F}_s, \hat{F}_v, \hat{v}_s, \hat{\delta}_\sigma\right] = [0.4186, 0.2709, 0.3222, 0.0702, 0.1112, 3.1972] \quad (22)$$

The presence of velocity fluctuations is evident, influencing the control command due to the use of a PID controller based on velocity error. In fact, the distribution of control inputs follows a pattern that can be approximated by a noisy linear regression with coefficient k_p. In addition, using the same dataset for parameter estimation, a spectral analysis of the velocity error $\omega_d - \omega$ is performed for each velocity set, as shown in Fig. 5. A correlation is observed between peak disturbances in the frequency domain and the reference velocity ω_d, which can be attributed to vibrations induced by the gearbox. Since the frequency of this disturbance is relatively low, any filtering action would introduce significant delays into the system, potentially leading to limit cycles.

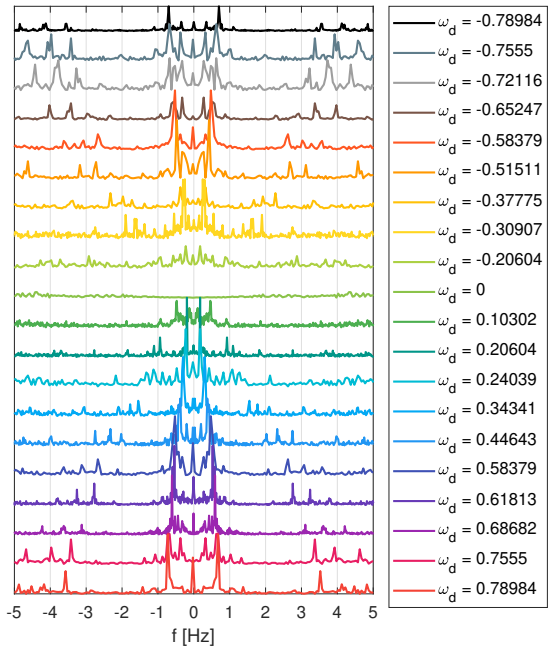

Fig. 5: Fourier analysis of the error ($\mathcal{F}(\omega_d - \omega)$)

Due to these factors, the estimated values represent the maximum possible reduction of asymmetries given the noisy nature of the system. Despite the influence of highly nonlinear effects on the estimation, Fig. 6 presents the identified friction model, which closely resembles the one in Fig. 1.

V. EXPERIMENTAL RESULTS

To evaluate the effectiveness of the proposed solution, a comparison is made between:

- the proposed switching PID controller;
- a standard PID position controller, as presented in (6);
- a cascade position-velocity PID controller;
  It is composed by two PID controller with respectively $(\vartheta_d - \vartheta) \to \omega_d$ *and* $(\omega_d - \omega) \to i$ *input-output transfer functions*;
- the state-of-the-art reset PID described in [5].
  For completeness, the flow diagram regulating the PID reset is shown in Fig. 7, with state machine parameters in Table IV.

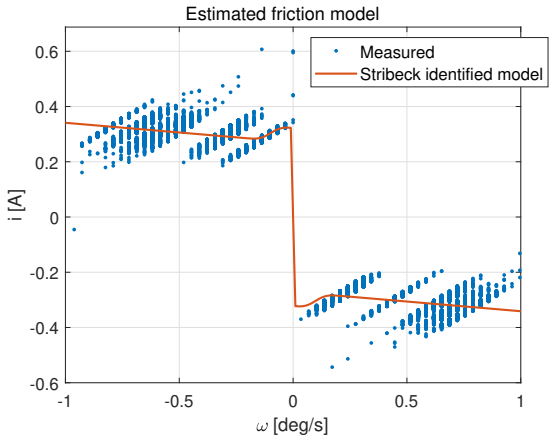

Fig. 6: Estimated friction model obtained during gravity compensation analysis - $\Psi(v, u_{vel,PID}) = u_{vel,PID} - k_g \cos(\vartheta)$

TABLE III: Common data and controller parameters

Common Data	
Sampling time (T_s)	0.01 s
Maximum current (i_{max})	2.0 A
Gravity compensation current (i_{grav})	$0.4186\cos(\vartheta)A$
Quantization position error ($\Delta\vartheta$)	$\approx 0.000343°$
Quantization velocity error ($\Delta\omega$)	$\approx 0.0343°/s$

Controllers	**In**	**Out**	k_p	k_i	k_d
Switching PID, PID, reset PID	e_ϑ	i	25	4.5	0.2
Cascade PID $e_\vartheta \to \omega_d$	e_ϑ	ω_d	30	2.0	0.1
Cascade PID $e_\omega \to i$	e_ω	i	0.5	1.0	0.0

To guarantee a fair comparison, all position controllers use the same gains and settings, as detailed in Table III.

The control performance is evaluated on a positioning task starting from the same initial positions, velocities and control actions. Without loss of generality, the desired position ϑ_d is set to zero. Results are presented in Fig. 8, where the position and the control action ϕ are reported. For the sake of readability, the control action is downsized by a

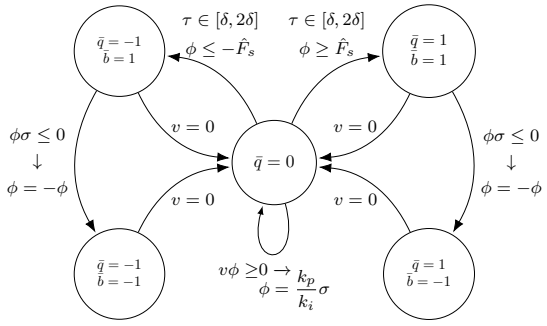

Fig. 7: Reset state machine proposed in [7]

factor of 100. As discussed in II-B, the position PID and the cascade position-velocity PID controls are unable to guarantee convergence to the desired position setpoint, as clearly visible in Figs. 8a-8b. The charge and discharge of integral action, which leads to hunting phenomena, can be observed from the control action signal. As expected, only the reset controller and the switching controller proposed in this paper can achieve the desired results. Despite this result, the performance of the two controllers differs significantly, as the switching PID allows convergence to the setpoint in approximately 10 seconds, whereas the reset PID takes 150 seconds. To explain this phenomenon, it is useful to note that, despite gravity compensation, friction remains slightly asymmetric between forward and downward movement and also varies during the same experiment. This phenomenon can be qualitatively assessed by observing the control action ϕ in Figs. 8a-8b: the system's motion is triggered by different control action values, indicating variations in static friction. This difference in performance between the two controllers can be justified by the fact that the reset PID assumes symmetry and consistency of the static friction.

For a more in-depth comparison, we evaluated the behavior of the reset PID for different tuning parameters. It is important to note that the switching PID has no tuning parameters other than the PID values, which are identical in both controllers. Interestingly, as shown in Fig. 9, tuning configurations 2 to 4 from Table IV fail to achieve system convergence. This is primarily due to two factors: an overestimation of static friction in at least one movement direction and an excessively high dwell-time. This confirms the importance of reducing the number of tunable parameters that depend on the model, further supporting the effectiveness of the proposed controller.

TABLE IV: Reset PID parameters

Parameters	**Tuning 1**	**Tuning 2**	**Tuning 3**	**Tuning 4**
Static friction ($\hat{F}_s$)	0.2	0.3	0.4	0.2
Dwell-time (δ)	0.05	0.05	0.05	0.1

Finally, Fig. 10 demonstrates the effectiveness of the proposed control action in handling both asymmetric friction phenomena and velocity measurement noise under different payload conditions. It is important to note that between experiments the gravitational compensation is not adjusted to account for load variations, leading to significant asymmetries. Despite these substantial variations in the static friction force across the three graphs, ranging from 0.5 A to 0.7 A for forward movement and from 0.2 A to 0.35 A for backward movement, the controller successfully drives the system to the desired state.

Additionally, Fig. 11 illustrates the scenario with the highest payload and where the initial condition is far from the setpoint, showing convergence to the desired state, as expected. This confirms that, despite this strong non linear disturbance and the velocity measurement noise, the controller is able to reach the desired setpoint.

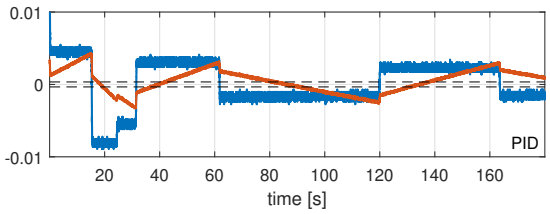

(a) PID

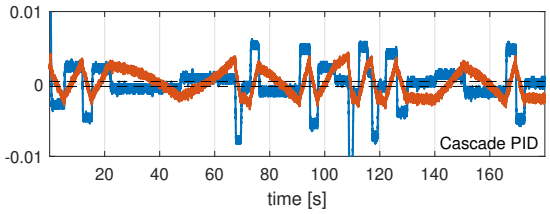

(b) Cascade PID

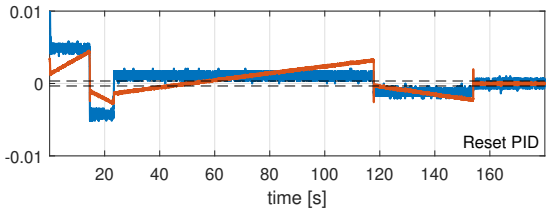

(c) Reset PID - Tuning 1

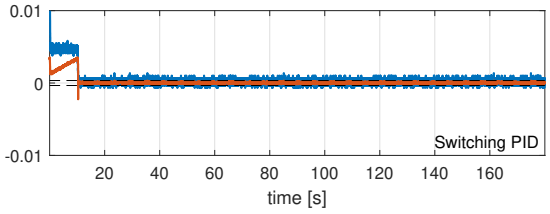

(d) Switching PID

Fig. 8: Experimental results comparison. There are shown the position ϑ (in blue) vs. the position tolerance $\pm\Delta\vartheta$ (dashed) and the control action $\phi/100$ (in orange).

VI. CONCLUSION AND FUTURE WORKS

In this paper, a control strategy for positioning systems affected by strongly asymmetric friction and noisy velocity measurements is proposed. This control action is based on a two-stage switching mechanism, which is formally proved, using hybrid Lyapunov arguments, to allow the system to converge to a steady state. The validation of the approach is performed through an experimental campaign on a real-world industrial setup, showing efficacy and robustness to static friction asymmetries and variations and to noise in the velocity measurements.

Future works will focus on extending the considered positioning scenarios, by including dynamic trajectories in the system behavior.

Manuscript 985 submitted to 2025 64th IEEE Conference on Decision and Control (CDC). Received March 31, 2025.

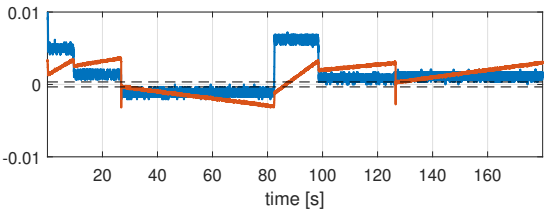

(a) Tuning 2

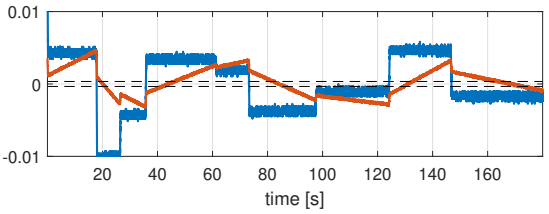

(b) Tuning 3

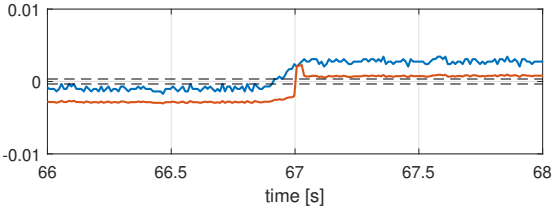

(c) Tuning 4

Fig. 9: Reset PID experimental results. There are shown the position ϑ (in blue) vs. the position tolerance $\pm\Delta\vartheta$ (dashed) and the control action $\phi/100$ (in orange).

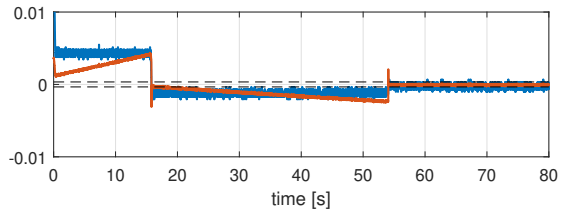

(a) No payload

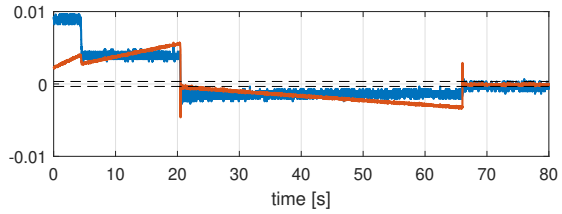

(b) Payload of 100 Nm

Fig. 10: Switching PID experimental results with different payload. There are shown the position ϑ (in blue) vs. the position tolerance $\pm\Delta\vartheta$ (dashed) and the control action $\phi/100$ (in orange).

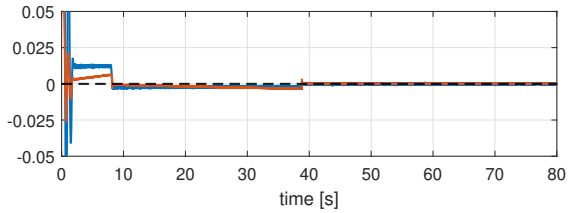

Fig. 11: Switching PID experimental results with different starting point and 200 Nm payload. There are shown the position ϑ (in blue) vs. the position tolerance $\pm\Delta\vartheta$ (dashed) and the control action $\phi/100$ (in orange).

Acknowledgment of Generative AI usage

During the preparation of this work, the authors used ChatGPT for light text editing. The authors take full responsibility for the content of the publication.

References

[1] Bajric, R., Sprečić, D., and Zuber, N. (2011). *Review of vibration signal processing techniques towards gear pairs damage identification*. *International Journal of Engineering & Technology IJET-IJENS*, Volume 11, Pages 124–128. [Online]. Available: https://api.semanticscholar.org/CorpusID:14111217

[2] Albert Wang and Sangbae Kim. *Directional efficiency in geared transmissions: Characterization of backdrivability towards improved proprioceptive control*. In *2015 IEEE International Conference on Robotics and Automation (ICRA)*, pages 1055–1062, 2015. doi:10.1109/ICRA.2015.7139307.

[3] H. Olsson, K. J. Åström, C. Canudas de Wit, M. Gäfvert, and P. Lischinsky. *Friction models and friction compensation*, *European Journal of Control*, vol. 4, no. 3, pp. 176–195, 1998. [Online]. Available: https://www.sciencedirect.com/science/article/pii/S094735809870113X.

[4] F. Marques, P. Flores, J.C. Claro, and H. Lankarani. *A survey and comparison of several friction force models for dynamic analysis of multibody mechanical systems*, *Nonlinear Dynamics*, vol. 86, pp. 1407-1443, Nov. 2016, doi: 10.1007/s11071-016-2999-3.

[5] R. Beerens, A. Bisoffi, L. Zaccarian, H. Nijmeijer, M. Heemels, and N. van de Wouw, *Reset PID Design for Motion Systems With Stribeck Friction*, *IEEE Transactions on Control Systems Technology*, vol. 30, no. 1, pp. 294–310, 2022. DOI: 10.1109/TCST.2021.3063420.

[6] D. Putra, H. Nijmeijer, and N. van de Wouw, *Analysis of undercompensation and overcompensation of friction in 1DOF mechanical systems*, *Automatica*, vol. 43, no. 8, pp. 1387–1394, 2007. DOI: 10.1016/j.automatica.2007.01.021. Available: ScienceDirect.

[7] A. Bisoffi, R. Beerens, W. P. M. H. Heemels, H. Nijmeijer, N. van de Wouw, and L. Zaccarian, *To stick or to slip: A reset PID control perspective on positioning systems with friction*, *Annual Reviews in Control*, vol. 49, pp. 37–63, 2020. DOI: 10.1016/j.arcontrol.2020.04.010. Available: ScienceDirect.

[8] A. Bisoffi, M. Da Lio, A. R. Teel, and L. Zaccarian, *Global asymptotic stability of a PID control system with Coulomb friction*, *IEEE Transactions on Automatic Control*, vol. 63, no. 8, pp. 2654–2661, 2018. DOI: 10.1109/TAC.2017.2774443.

[9] R. Beerens, A. Bisoffi, L. Zaccarian, H. Nijmeijer, M. Heemels, and N. van de Wouw, "*Reset PID design for motion systems with Stribeck friction*, *IEEE Transactions on Control Systems Technology*, vol. 30, no. 1, pp. 294–310, 2022. DOI: 10.1109/TCST.2021.3063420.